PCCP

ROYAL SOCIETY OF CHEMISTRY

PAPER

View Article Online
View Journal | View Issue

Check for updates

Cite this: *Phys. Chem. Chem. Phys.*, 2025, **27**, 83

Don't forget the *trans*: double bond isomerism radical-acetylene growth reactions affect the primary stages of PAH and soot formation†

Patricia D. Kelly, *[a] Jack A. Turner,[a] Oisin J. Shiels,[a] Gabriel da Silva, [b] Stephen J. Blanksby, [c] Berwyck L. J. Poad [c] and Adam J. Trevitt *[a]

In combustion, acetylene is a key species in molecular-weight growth reactions that form polycyclic aromatic hydrocarbons (PAHs) and ultimately soot particles. Radical addition to acetylene generates a vinyl radical intermediate, which has both *trans* and *cis* isomers. This isomerism can lead to profound changes in product distributions that are as yet insufficiently investigated. Herein, we explore acetylene addition to substituted *trans*-vinyl radicals, including potential rearrangement to *cis* structures, for eight combustion-related hydrocarbon radicals calculated using a composite method (G3X-K). Of these eight systems, the phenyl *trans*- and *cis*-Bittner–Howard HACA (hydrogen abstraction, C_2H_2 Addition) process, where acetylene successively adds to a phenyl radical *via* a β-styryl intermediate, is simulated using a unified Master Equation model. Including the *trans*-Bittner–Howard pathway changes the products significantly at all simulated temperatures (550–1800 K) and pressures (5.33×10^2–10^7 Pa), relative to a *cis*-only model. Typically, naphthalene remains the dominant product, but its abundance decreases at higher temperatures and pressures. For example, at 1200 K and 10^5 Pa, its branching ratio decreases from 78.5% to 62.9% when the *trans* pathway is included. At higher temperatures this decrease corresponds to the formation of alternative $C_{10}H_8$ isomers, including the *cis* product benzofulvene with 8% maximum abundance at 1200 K and 5.33×10^2 Pa, and *E*-2-ethynyl-1-phenylethylene, a *trans* product with 26% maximum abundance at 1800 K, with little pressure dependence. At higher pressures, our model predicts a range of $C_{10}H_9$ radicals, including resonance-stabilised radicals (RSRs). The impact of *trans*-vinyl radical chemistry in reactive environments means that they are essential to accurately describe combustion reactions and inhibit soot formation.

Received 13th September 2024,
Accepted 27th November 2024

DOI: 10.1039/d4cp03554b

rsc.li/pccp

Introduction

Molecular-weight growth radical chemistry is central to understanding combustion chemistry and it results in the formation of polycyclic aromatic hydrocarbon (PAH) species that eventually seed the formation of soot particles. Both PAHs and soot particles are widely known to contribute strongly to the negative health impact of polluted air[1–4] – so accurate models are crucial to predict and mitigate these impacts. Although the process of soot formation by molecular-weight growth has been qualitatively understood for decades,[5–8] the precise chemical mechanisms remain a focus of contemporary experimental and computational research.[4,7–9]

As computational methods have increased in power, a greater scope of chemical species have been included in models of hydrocarbon molecular-weight growth.[7,8,10–17] Numerous models implicate the reaction between a hydrocarbon radical and an unsaturated closed–shell co-reactant, such as acetylene.[18–20] Acetylene is one of the most abundant small hydrocarbons implicated in the formation of larger species.[6,21] Radical addition to the acetylene triple bond yields odd-electron adducts with a vinyl (sp^2) radical that can interconvert between *trans* and *cis* isomeric forms. Scheme 1 shows an example of such an adduct, the β-styryl radical, which has *trans* (*Z*-βS)‡ and *cis* (*E*-βS) forms that can easily isomerise. However, as shown in Scheme 1, when a second acetylene molecule adds to the radical intermediate, any subsequent *trans*/*cis* isomerism

---

[a] *School of Chemistry and Molecular Bioscience, University of Wollongong, Wollongong, NSW, Australia. E-mail: paddy@uow.edu.au, adamt@uow.edu.au*

[b] *Department of Chemical Engineering, The University of Melbourne, Melbourne, Victoria, Australia*

[c] *Central Analytical Research Facility and the School of Chemistry and Physics, Queensland University of Technology, Brisbane, Queensland, Australia*

† Electronic supplementary information (ESI) available. See DOI: **https://doi.org/10.1039/d4cp03554b**

‡ The *trans* form is *Z* in this case as the radical site has lower priority than the H atom.

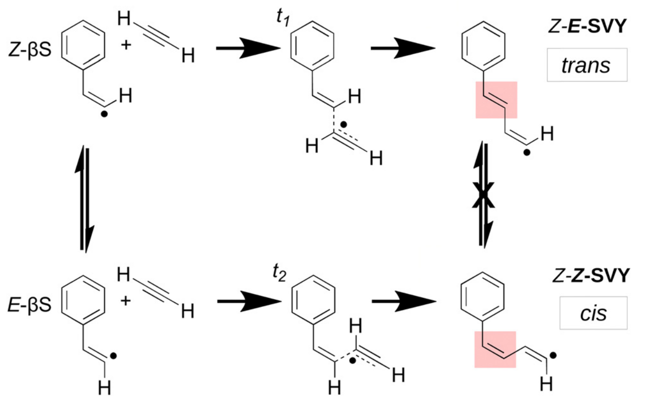

Scheme 1 Acetylene addition to both (*trans*) *Z*- and (*cis*) *E*-β-styryl radicals *via* transition states t_1 and t_2, beginning the *trans* and *cis*-Bittner–Howard pathways. *Z*- and *E*-β-styryl radicals can rapidly interconvert by the movement of one hydrogen atom, whereas the adducts are unable to easily isomerise *via* rotation of the highlighted double bond.

between the *trans* *Z*-***E*-SVY** and the *cis* *Z*-***Z*-SVY** is "locked out" by the high rotational barrier of the double bond. This effect has been noted for vinyl radicals in the solution phase, where differences in reactivity between *trans* and *cis* isomers are often observed.[22,23] Though many acetylene-radical reactions feature *trans* and *cis* vinyl radical adducts, including the Bittner–Howard pathway in the well-known hydrogen abstraction, C_2H_2 addition (HACA) mechanism, few studies have explicitly examined pathways leading from the *trans* reactive intermediate.[5,24,25]

Scheme 2 shows the general phenyl HACA mechanism, long considered the key process for the growth of benzene to naphthalene and beyond in flames. This mechanism comprises multiple pathways; among these are the Bittner–Howard, Frenklach and modified Frenklach pathways.[5,6,25,26] Both the Bittner–Howard and modified Frenklach pathways involve secondary C_2H_2 addition to a C_8H_7 radical isomer. Recent work by Mebel *et al.* argues that these pathways are unrealistic under typical low-pressure flame conditions due to the instability of C_8H_7 radicals above 1650 K at 1 atm, leading to a low equilibrium concentration of C_8H_7 relative to C_6H_5 + C_2H_2.[25] Experiments and further modelling by Green *et al.*[27] focused specifically on these low-pressure, low-temperature conditions, and predicted that *ca.* 70% of naphthalene produced in the HACA reaction arises *via* the Bittner–Howard pathway at 700 K, 10 torr at a reaction time of 1 ms. However, modelling by Green *et al.* of the Bittner–Howard pathway incorporated the radical intermediates calculated by Mebel *et al.*, but these did not appear to include the *trans*-Bittner–Howard pathway.

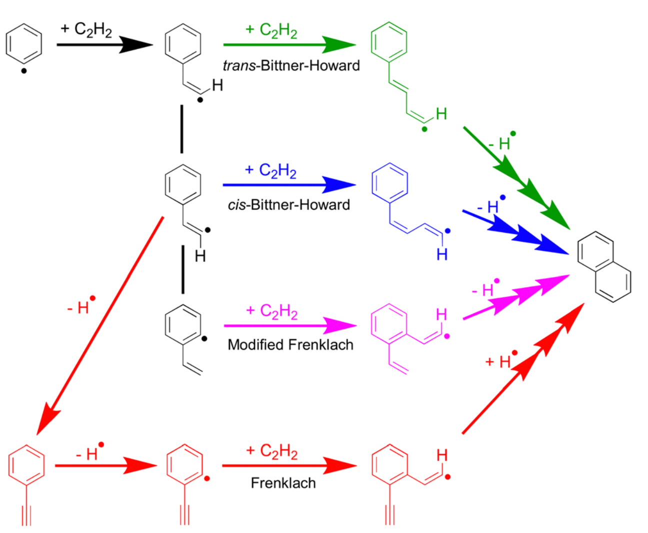

Scheme 2 Simplified pathways of the general phenyl HACA mechanism. Green is *trans*-Bittner–Howard, blue is *cis*-Bittner–Howard, pink is modified Frenklach and red is Frenklach. Ring closing in the green pathway is inhibited by the high barrier for rotation about the double bond. Multiple-headed arrows indicate a pathway with multiple intermediates.

An important class of molecules in combustion and soot formation are resonance-stabilised radicals (RSRs) and these readily react with other radicals or closed-shell species, while also being relatively long-lived.[4,7,8,28–30] The prior work by Mebel[25] predicts a variety RSRs arising from HACA reactions, including hydronaphthyl RSRs from both the *cis*-Bittner–Howard and modified Frenklach pathways. However, within the *cis*-Bittner–Howard mechanism the only RSR present is an intermediate that leads directly to naphthalene formation, and is only predicted to have significant yield at 100 atm and temperatures below *ca.* 1000 K. At the lower pressures studied by Green *et al.*, naphthalene is expected to form *via* so-called "formally direct" pathways, involving well-skipping over RSR intermediates due to the lack of collisional stabilisation.[27] Such well-skipping to form naphthalene is not possible in the *trans*-Bittner–Howard pathway,[24,25] however, and this indicates that the inclusion of this pathway may have a large effect on product branching ratios.

In this paper, a detailed theoretical reaction rate model and analysis of both the *trans*- and *cis*-Bittner–Howard HACA pathways is reported for an extensive set of $C_{10}H_9$ and $C_{10}H_8$ isomers. Branching ratios for all intermediates and products are reported at temperatures from 550 to 1800 K, and pressures from 5.33×10^2 to 10^7 Pa. An important conclusion of this paper is that *trans*/*cis* isomerism has a significant outcome on predicted branching ratios over large temperature and pressure ranges, and compared with prior modelling the $C_{10}H_9$ RSRs and alternative $C_{10}H_8$ isomers (such as benzofulvene) are much more abundant.

Methods and model description

Simulation of the *trans*- and *cis*-Bittner–Howard pathways was achieved using a master equation (ME) model within the MultiWell 2020 program.[31–33] The model contains 38 intermediate $C_{10}H_9$ minima (or wells), 78 transition states and 10 dissociation channels including the 2 possible entry channels. This model is a more comprehensive simulation of the secondary reaction than previously published studies. Gaussian 16[34] was used to calculate the electronic energy of each structure at the G3X-K level of theory,[35] with transition states located by redundant coordinate scans and verified by visual inspection of the imaginary frequency. In cases where visual inspection alone could not unambiguously identify connectivity of minima and transition states, intrinsic reaction coordinate (IRC) calculations were also used to confirm this connectivity. The same model chemistry was also used to calculate a *trans* pathway for a broad variety of acetylene-radical reactions.

RRKM theory is adopted for $k(E)$ calculations, on the basis of sums and densities of states. To calculate the density of states for each stationary point, a RRHO (rigid rotor + harmonic oscillator) model was augmented with hindered rotor potentials to replace the harmonic oscillator descriptions for sufficiently facile bond rotations. Hindered rotor potentials were calculated using relaxed coordinate scans with a step size of 10 degrees. The energies at each point were then fit with a Fourier series comprising nineteen cosine and sine terms. Moments of inertia were estimated at a single point. Collisional energy transfer was described using a single-exponential-down model with parameters based on those of toluene in a He bath gas.[36,37] Toluene was chosen as it is a chemically similar species to most of the $C_{10}H_9$ isomers with established parameters, and the effect of altering these parameters is less significant than the uncertainty introduced by errors in the relative energies.[25]

In total, sixty different sets of initial conditions were simulated, with each simulation including 10^7 Monte Carlo trials. These conditions described the reaction at six different temperatures between 550 K and 1800 K, and five different pressures between 5.33×10^2 Pa (4 torr) and 10^7 Pa (7.5×10^4 torr), for two different initiating reactions. The lowest pressure and temperature values were chosen to correspond to concurrent photoionisation mass spectrometry experiments,[38] discussed in the ESI† and to be further detailed in a future publication. The initial formation of both *trans* and *cis* isomers was incorporated by running simulations starting as chemically activated populations of both initial wells, which can subsequently interconvert, isomerise and dissociate independently. Each of the sixty total simulations were calculated to 1000 collisions, which was sufficient for most of the excess energy to be dissipated or to completely dissociate the $C_{10}H_9$ intermediates. Tertiary addition of another acetylene molecule was deemed to be negligible on this timescale. Species with an sp^2 radical and an α-hydrogen were summed together after calculation due to the very low interconversion barrier between these species. Following ref. 39 and 40, we assume that intramolecular vibrational energy redistribution (IVR) is complete in less than a few picoseconds.

To determine the relative contribution of the *trans* and *cis* pathways to the overall reaction, the partition functions for entry transition states t_1 and t_2 were calculated, as labelled in Scheme 1. Transition state theory provides the following equation:[41]

$$k(T) = F_w Z_t(T) e^{-\beta E_t}$$

where k is the reaction rate, Z_t is the partition function of the transition state, β is the thermodynamic beta, E_t is the energy of the transition state, and F_w is some function that depends only on the initial well or separated reactants. If it is assumed that both *trans* and *cis* pathways can interconvert rapidly prior to the crossing of one of two transition states, the prefactor F_w can be ignored when calculating the branching ratio. This allows a simple means for its estimation without specific knowledge of any pre-reactive complex. This relation only breaks down if acetylene is abundant enough that the *trans* and *cis* isomers of C_8H_7 do not have time to equilibrate before a reactive collision occurs, which would likely only occur at high number densities well beyond those simulated in this work.

Results and discussion

This first section contains a general overview analysis of *trans*/*cis* isomerism chemistry of vinyl radical intermediates involved in acetylene molecular-weight growth chemistry considering a range of fundamental combustion-related hydrocarbon radicals. Of these radicals, the reaction of the phenyl radical with acetylene *via* the Bittner–Howard pathway was selected for further analysis using a detailed ME model spanning a range of pressure and temperatures, and this is examined in more detail further below. With this detailed ME model at hand, the branching ratio of each species was calculated as a function of pressure and temperature – this allows for comparison to previous studies in the literature. Finally, the contribution of the *trans* pathway is assessed by calculating the change in branching ratio when it is included and compared with when it is omitted.

The *trans*/*cis* isomerism in hydrocarbon radical-acetylene reactions

As a starting point, to assess the significance of the *trans* reaction within the context of acetylene molecular-weight growth reactions, a series of analogous pathways across a range of fundamental hydrocarbon radicals were calculated using the G3X-K method, and these are shown together in Fig. 1. This figure depicts the energy landscape for the catalytic vinylacetylene formation pathway for the RSRs propargyl ($CHCCH_2$) and allyl (CH_2CHCH_2), together with selected saturated (methyl (CH_3), ethyl (C_2H_5) and propyl (C_3H_7)) and unsaturated (ethenyl (CH_2CH), phenyl (c-C_6H_5) and ethynyl (C_2H)) non-resonance-stabilised radicals. As these pathways do not involve significant R-group interactions, it is a reasonably straightforward comparison. Fig. 1(a) depicts the energy of the primary addition (n = 1) of acetylene to the radical, which forms the adduct complex *via* a single transition state. For most cases, the transition-state energy is positive with respect to the separated reactants, except for the ethynyl radical case, which is slightly submerged. Fig. 1(b) is a portion of the secondary (n = 2) addition of acetylene to the primary radical adduct. This n = 2 pathway contains a series of H atom shifts, followed by an interconversion between linear and branched isomers that form *via* a three-membered cyclic intermediate. If viable, this pathway is an alternative pathway to form vinylacetylene, rather

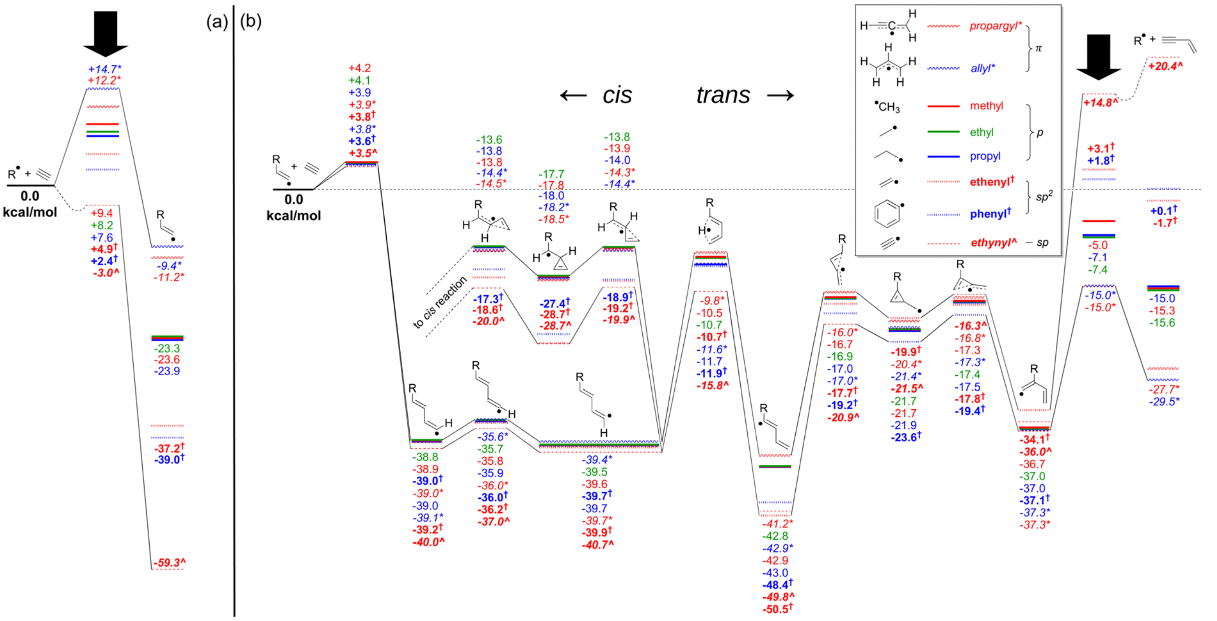

Fig. 1 G3X-K energetics, in kcal mol^{-1}, of selected pathways of (a) primary, and (b) *trans* secondary addition to various radicals. Catalytic vinylacetylene generation progresses to the right, competing with the isomerisation pathway to the *cis* reaction branching back to the left (the products of which are not shown). Solid arrows indicate the initial formation and final dissociation step. The colours, symbols and text styles are matched to the radical species depicted in the legend. Dotted wells in the adduction or fragmentation step indicate the existence of a pre- or post-reactive complex, the calculation of which was outside the scope of this study.

than from the reaction of liberated H atoms with acetylene.[42] Across both Fig. 1(a) and (b), most intermediates and transition states have relative energies that do not strongly depend on the R group. The differences between each case are most apparent for the primary addition step (Fig. 1(a)) and in the final regeneration of the starting radical (Fig. 1(b)). These points are marked with a black downward arrow, and their spread in energy values is attributed to the varying radical stabilisation energies (RSEs) of each radical, with relatively stable conjugated radicals such as allyl and propargyl having the largest RSE values.[43] More localised radicals such as ethynyl, and to a lesser extent ethenyl (vinyl) and phenyl, exhibit the opposite trend and have the highest values. Indeed, Fig. 1(b) shows similar $n = 2$ energetics across all R groups as the $n = 1$ adduct always bears an sp^2 radical site, and therefore the RSE for each adduct is similar. Furthermore, intermediates along the catalytic vinylacetylene formation pathway have similar energy (relative to their respective $n = 1$ adducts separated from acetylene), as the interaction with the R group is in most cases quite limited.

The primary isomerisation step that connects the *trans* to the *cis* pathway also involves a three-member cyclic intermediate and is also only weakly affected by the R-group. Of these, the highest-energy barrier resides between −13.6 and −20.0 kcal mol^{-1}, relative to the separated reactants. The small differences are mostly attributed to resonance stabilisation of the aforementioned three-member cyclic intermediate in cases where the precursor radical site is sp^2 or sp (*e.g.* the phenyl radical), which does not occur for p- or π-type precursor radicals. Therefore, this pathway is more facile in the phenyl case than for most others. Nonetheless, in all cases the three-member cyclic intermediate geometry likely indicates a low density of vibrational states – and so entropic effects may allow higher-energy *trans* pathways to remain relevant. If these entropic effects allow the *trans* reaction to contribute significantly even in cases where the interconversion is stabilised, such as for the phenyl radical in the Bittner–Howard pathway, our recommendation is that it must also be included for the non-stabilised cases.

Since the reactions of the phenyl radical (the solid blue pathway in Fig. 1) are implicated in many soot formation models, this pathway is selected for further scrutiny and modelled in detail. To ascertain if the *trans* pathway of the Bittner–Howard reaction leads to significantly different products, a detailed chemical model is presented below, with branching ratios assessed as a function of pressure, temperature, and *trans*/*cis* isomerism.

Product formation in the Bittner–Howard reaction

The simplest definition of the Bittner–Howard reaction is a naphthalene-forming reaction between phenyl and acetylene where a second acetylene adds to a β-styryl radical (Scheme 1). In this section, we expand this definition to include the full surface and range of products for the reaction of the β-styryl radical with acetylene. This broader scope includes the *trans*- and *cis*-Bittner–Howard variants that depend on the stereoisomerism of the β-styryl radical site. Together, these variants comprise a significant portion of the $C_{10}H_9$ surface. Fig. 2 presents all minima, transition states, reactants and products of this surface modelled in this work. The starting β-styryl

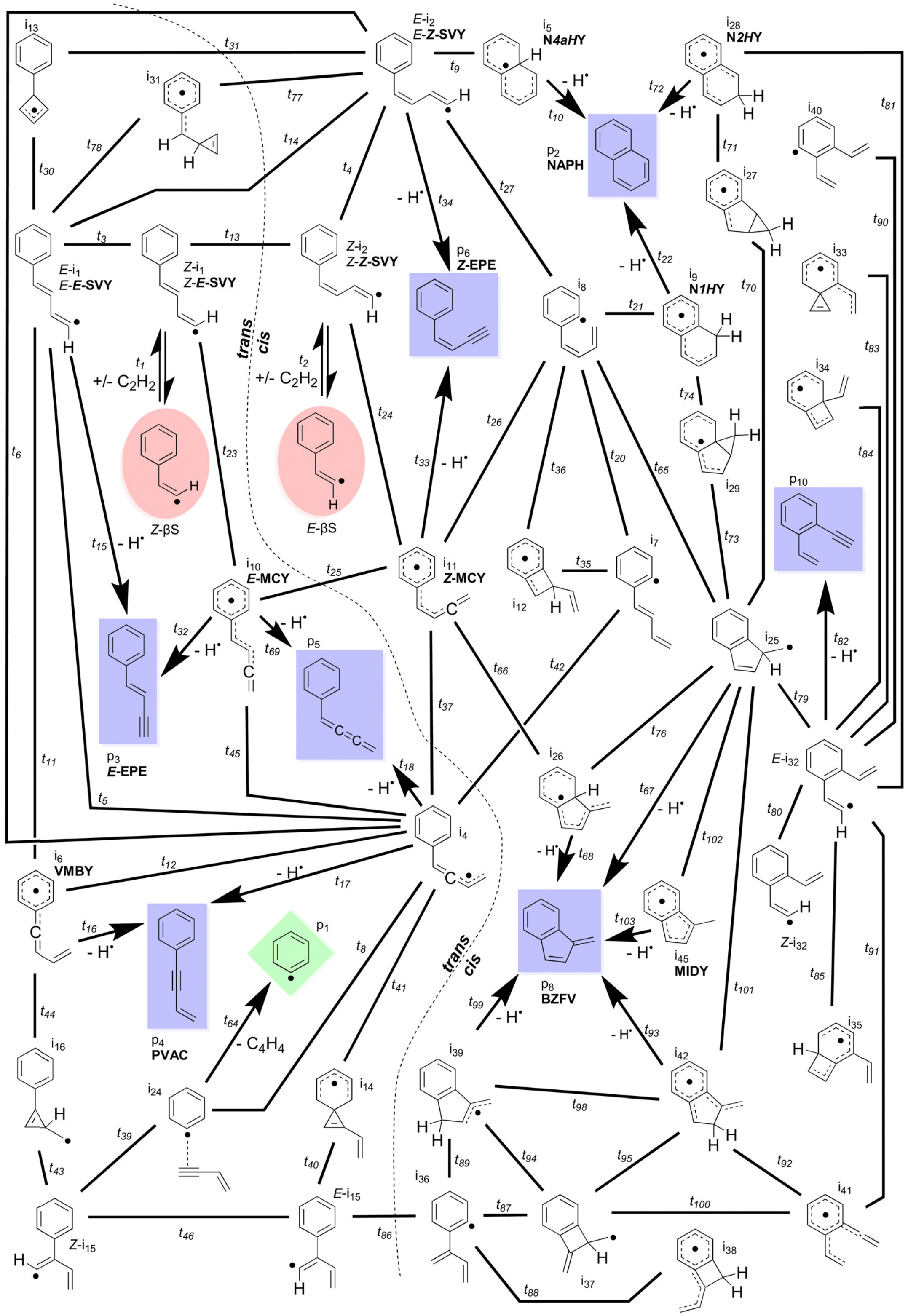
i_{13}
t_{31}
E-i_2
E-Z-SVY
t_9
i_5
N4aHY
i_{28}
N2HY
i_{31}
t_{77}
- H•
t_{72}
- H•
t_{10}
t_{81}
i_{40}
t_{78}
t_{14}
t_{30}
t_4
p_2
NAPH
t_{71}
- H•
t_{34}
t_{27}
i_{27}
t_{90}
t_3
t_{13}
E-i_1
E-E-SVY
Z-i_1
Z-E-SVY
Z-i_2
Z-Z-SVY
p_6
Z-EPE
- H•
t_{22}
i_9
N1HY
i_8
t_{21}
t_{70}
i_{33}
trans
cis
t_1
+/- C_2H_2
t_2
+/- C_2H_2
t_{83}
i_{34}
t_{74}
t_6
t_{23}
t_{24}
t_{26}
t_{36}
t_{20}
t_{65}
i_{29}
t_{84}
p_{10}
Z-βS
E-βS
t_{33}
- H•
t_{15}
- H•
i_{10}
E-MCY
t_{25}
i_{11}
Z-MCY
t_{35}
i_7
i_{12}
t_{73}
t_{32}
- H•
t_{69}
- H•
p_5
i_{25}
t_{82}
- H•
t_{66}
t_{42}
t_{37}
t_{79}
t_{11}
p_3
E-EPE
t_{45}
t_{76}
i_{26}
t_{18}
- H•
t_5
E-i_{32}
t_{67}
- H•
t_{80}
i_4
t_{102}
- H•
t_{68}
i_6
VMBY
t_{12}
- H•
t_{17}
Z-i_{32}
t_{103}
- H•
p_1
t_{16}
- H•
t_8
trans
cis
i_{45}
MIDY
t_{91}
t_{44}
p_4
PVAC
t_{64}
- C_4H_4
t_{41}
t_{99}
- H•
p_8
BZFV
t_{101}
t_{85}
- H•
t_{93}
i_{16}
i_{24}
i_{14}
i_{39}
i_{42}
i_{35}
t_{98}
t_{39}
t_{43}
t_{40}
t_{89}
t_{94}
t_{95}
t_{92}
i_{36}
E-i_{15}
t_{87}
t_{100}
i_{41}
Z-i_{15}
t_{46}
t_{86}
i_{38}
t_{88}
i_{37}

Fig. 2 Full network of the modelled intermediates, transition states and exit channels of the $C_{10}H_9$ surface in the Bittner–Howard reaction. Each bold line corresponds to an isomerisation transition state, with arrows depicting attachment and/or detachment. The starting β-styryl C_8H_7 isomers are enclosed in red ellipses, $C_{10}H_8$ isomers in blue rectangles, and C_6H_5 in a green diamond. A dotted line approximately divides the *trans*- (left) and *cis*-Bittner–Howard (right) pathways. Intermediates and products discussed in the text are labelled with a bold abbreviation, *e.g.* **NAPH**.

radicals are enclosed in red ellipses. For each of these points, the energy relative to separated reactants is provided in the ESI† (Table S2). The left side of Fig. 2 is the *trans* pathway, with the *cis* pathway on the right (separated by the dashed curved line).

Nine connecting transition states are noted between the *trans* and *cis* pathways, most of which are high in energy or are linked to uncommon intermediates. These transition states involve rotation about the α–β bond, either directly or *via* an intermediate. Once one of the two adducts form, several rearrangements can take place – the most important of which are shown in more detail later. Some rearrangements lead to dissociation, either to re-form the β-styryl radicals, H-loss ($C_{10}H_8$) products (blue rectangles), or the previously described vinylacetylene loss pathway (green diamond). Intermediates and products discussed in the text are labelled with a bold abbreviation.

The points on the surface described in Fig. 2 form the basis of the ME model described in this work, which predicts branching ratios for each species. Of the thirty-four $C_{10}H_9$ intermediates and seven $C_{10}H_8$ products, Scheme 3 lists the fourteen most abundant in the ME model. These species include bicyclic or monocyclic structures, with the bicyclic radicals resulting from the *cis* pathway, and the monocyclic species mostly from the *trans* pathway. Aside from the closed–shell $C_{10}H_8$ isomers (top), various open–shell $C_{10}H_9$ species are present, including both of the $n = 2$ adducts as well as a variety of RSRs. The variation in branching ratios of these species under different conditions is discussed below.

Naphthalene and other $C_{10}H_8$ isomers. Given a pressure and temperature, the model presented in this paper provides branching ratios for all included species. Thus, by varying pressure and temperature, the branching ratio for a particular species can be depicted across these physical conditions. Fig. 3 shows the predicted branching ratios of various $C_{10}H_8$ species as a function of pressure and temperature – with colour indicating the value of the branching ratio at the pressures and temperatures indicated by the crosses. These values, as well as those for all other species, are tabulated in the ESI† (Table S3). At the lowest pressures and temperatures, in accord with the previous study by Mebel *et al.*,[25] the production of naphthalene (**NAPH**) is the dominant result looking at the bottom left-hand corner across each of the four panels in Fig. 3. However, at pressures beyond 10^4 Pa, or temperatures exceeding 800 K, other pathways become significant as the **NAPH** branching ratio drops. In particular, at 550 K and 10^5 Pa, the **NAPH** branching ratio falls to 58.5%, and at 1000 K and 5.33×10^2 Pa, it falls to 76.5%. When temperature increases to 1500 K (at 5.33×10^2 Pa), **NAPH**'s branching ratio decreases to 40.7%, and by 1800 K it is no longer the main product. Though Mebel *et al.* also predict a reduction in **NAPH** branching ratio at high pressure and temperature, their yield is always

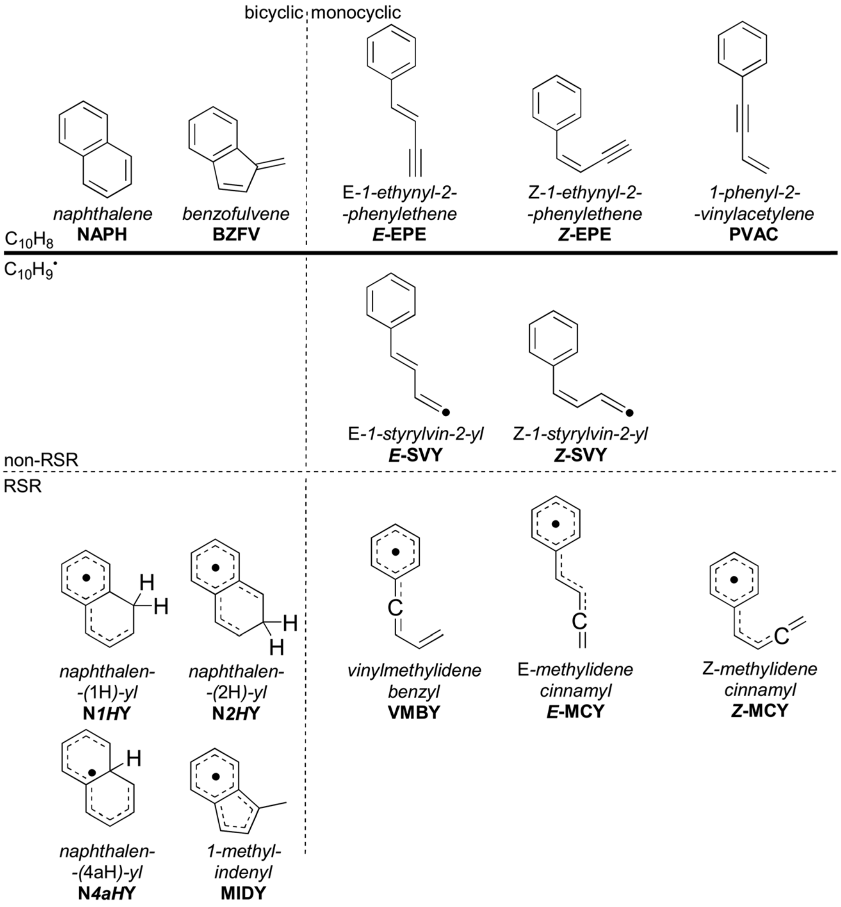
bicyclic
monocyclic
$C_{10}H_8$
naphthalene
NAPH
benzofulvene
BZFV
E-1-ethynyl-2--phenylethene
E-EPE
Z-1-ethynyl-2--phenylethene
Z-EPE
1-phenyl-2--vinylacetylene
PVAC
$C_{10}H_9^{\bullet}$
E-1-styrylvin-2-yl
E-SVY
Z-1-styrylvin-2-yl
Z-SVY
non-RSR
RSR
H
H
naphthalen--(1H)-yl
N1HY
naphthalen--(2H)-yl
N2HY
C
vinylmethylidene benzyl
VMBY
E-methylidene cinnamyl
E-MCY
Z-methylidene cinnamyl
Z-MCY
naphthalen--(4aH)-yl
N4aHY
1-methyl-indenyl
MIDY

Scheme 3 Modelled species with a branching ratio exceeding 1% in any set of simulated pressure and temperature conditions, including the abbreviations used in the text. Species are divided by mass, number of rings, and presence of resonance-stabilised radical sites.

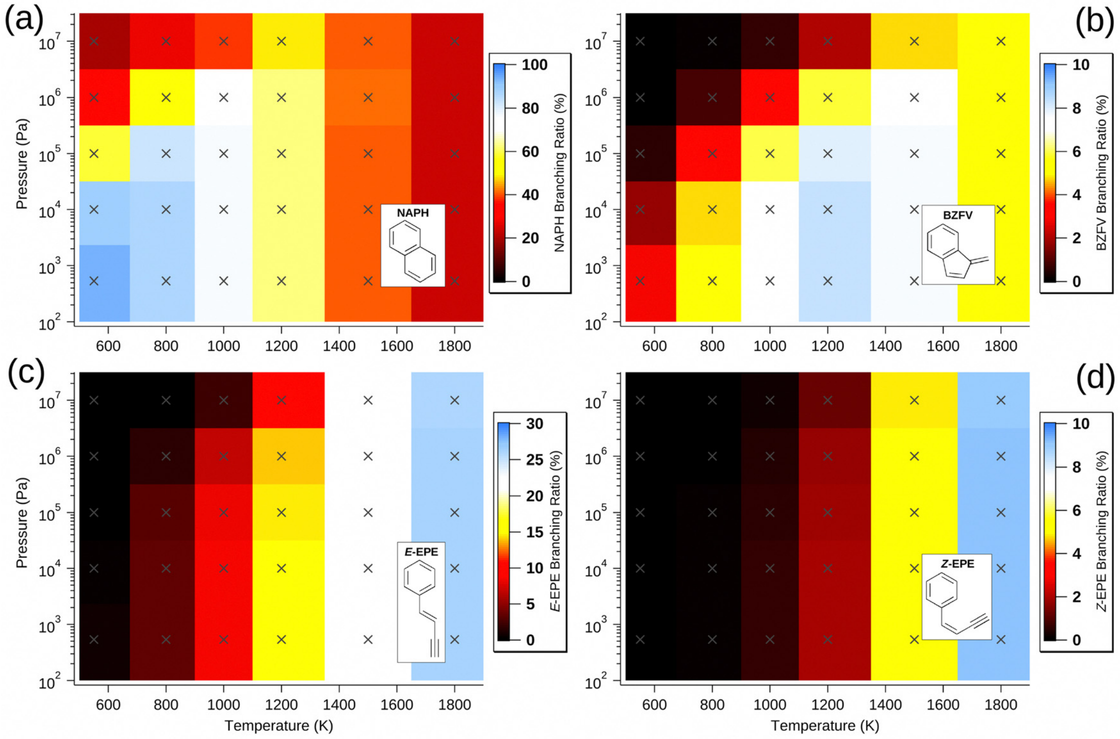

Fig. 3 Predicted branching ratio of (a) **NAPH**, (b) **BZFV**, (c) ***E*-EPE** and (d) ***Z*-EPE**, as a function of pressure and temperature. Crosses designate points at which the model was calculated. Colour is used to indicate the value of the branching ratio at these pressure and temperature coordinates – note that the intensity scales are different for each plot.

above 80% until the pressure exceeds 10^6 Pa or the temperature is above 2000 K – and at low pressure, is always the majority product even at 2500 K.[25] At high temperatures, we find that much of the reduction in **NAPH** branching ratio results from the increasing formation of *E*-1-ethynyl-2-phenylethylene (***E*-EPE**, Fig. 3(c)), which is a *trans* species not explicitly included in previous studies. The formation of ***E*-EPE** has only a weak dependence on pressure but increases to a maximum value of *ca.* 26% at 1800 K. Formation of the corresponding *cis* isomer, *Z*-1-ethynyl-2-phenylethylene (***Z*-EPE**, Fig. 3(d)), also varies only weakly with pressure, but only reaches a maximum branching ratio of *ca.* 9% at 1800 K, which is comparable with previous studies.

Though most non-**NAPH** $C_{10}H_8$ isomers are produced in greater abundance as temperature increases, with only a weak pressure dependence, benzofulvene (**BZFV**) is most prevalent at low pressure and intermediate temperature and this is due to its production from the *cis*-Bittner–Howard pathway and its relative stability compared to the monocyclic isomers. Since it is a product of the *cis* pathway along with **NAPH**, **BZFV** is formed under generally similar conditions, but the lower threshold energy for formation of **NAPH** relative to **BZFV** results in preference for the former at the lowest temperatures. However, the integrated density of states of **BZFV** grows more rapidly than that of **NAPH** as temperature increases, somewhat offsetting this effect at higher temperature. At conditions of 5.33×10^2 Pa and 1200 K, **BZFV** has a predicted branching ratio exceeding 8% – despite not appearing to be implicated in previous studies.

$C_{10}H_9$ intermediates and vinylacetylene. Although this high temperature/high pressure reduction in **NAPH** production compared with previous reported models is attributed to the formation of other $C_{10}H_8$ isomers at high temperatures, at low temperature (and high pressure) much of this reduction in **NAPH** production results from the stabilisation of $C_{10}H_9$ radical intermediates. Fig. 4 shows the branching ratio as a function of pressure and temperature for some of these $C_{10}H_9$ intermediates, including *E*-1-styrylvin-2-yl (***E*-SVY**) and methylindenyl (**MIDY**). Under most conditions, ***E*-SVY** (Fig. 4(a)) is by far the most produced $C_{10}H_9$ radical intermediate, with a branching ratio of total species of *ca.* 59% at 550 K and 10^7 Pa. ***E*-SVY** is almost exclusively the result of a collision-stabilised *trans*-Bittner–Howard pathway, and is much more common than its isomer *Z*-1-styrylvin-2-yl (***Z*-SVY**), which does not exceed *ca.* 3% at these conditions.

Aside from the ***E***- and ***Z*-SVY** adduct radicals, all of the radical intermediates that are present in appreciable (>1%) quantities are RSRs. These are vinylmethylidene benzyl (**VMBY**), **MIDY**, naphthalen-(1*H*)-yl (**N1*H*Y**), naphthalen-(2*H*)-yl (**N2*H*Y**), naphthalen-(4a*H*)-yl (**N4a*H*Y**), *E*-methylidene cinnamyl (***E*-MCY**) and *Z*-methylidene cinnamyl (***Z*-MCY**) and Fig. 4(b) shows the total branching ratio for these and all other RSRs summed together. Together, these RSRs comprise 18% of all products at 10^7 Pa and 800 K. Generally, as expected, higher pressure and lower temperature are conditions that favour these species, as with all $C_{10}H_9$ radicals in the model. However, the dependence on both pressure and temperature is much weaker than for ***E***- and ***Z*-SVY**. RSRs are

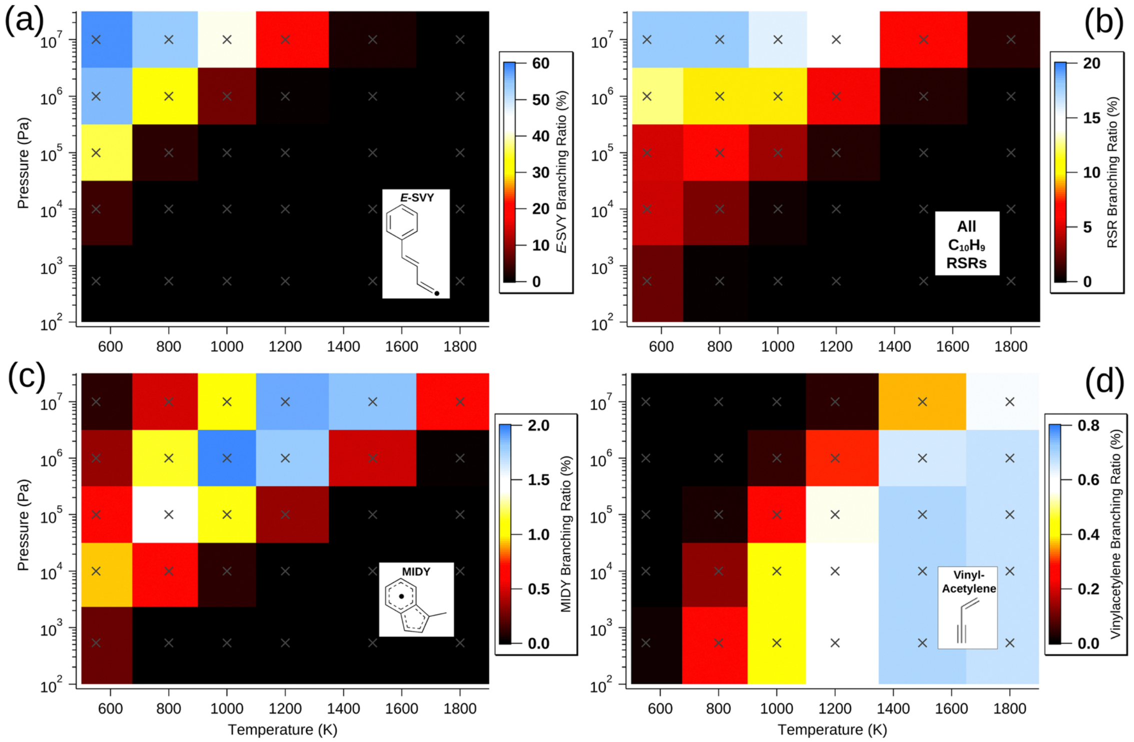

Fig. 4 Predicted branching ratio of (a) ***E*-SVY**, (b) all RSRs, (c) **MIDY** and (d) vinylacetylene (with phenyl co-fragment), as a function of pressure and temperature. Crosses designate points at which the model was calculated. Colour is used to indicate the value of the branching ratio at these pressure and temperature coordinates – note that the intensity scales are different for each plot.

present at abundances exceeding 1% for sixteen of the thirty simulated pressures and temperatures, indicating that the Bittner–Howard pathway may often contribute to RSR-based molecular-weight growth.

Of note among RSRs is also **MIDY**, shown in Fig. 4(c). **MIDY** is a substituted indenyl radical – the indenyl radical is much less prone to decomposition at intermediate temperatures compared with many other fuel-derived radicals.[30] Indenyl radicals have been studied as a target for RSR-based molecular-weight growth,[4,8,30] and therefore the formation of **MIDY** in the Bittner–Howard pathway should not be overlooked. Interestingly, **MIDY** is less present *ca.* 550 K and 10^7 Pa, likely due to the many-step process required for its formation and competition with other radicals that are more stable at lower temperature. Though our analysis predicts **MIDY** has a branching ratio of only a few percent at most, its relative persistence at higher temperatures indicates that the Bittner–Howard pathway in the phenyl HACA reaction can contribute to RSR-based molecular-weight growth even under these conditions.

A minor channel that is neither $C_{10}H_8$ nor $C_{10}H_9$ is the loss of vinylacetylene to regenerate phenyl radicals. As discussed above, this bimolecular product channel is the *trans*-specific final step of a radical-catalysed acetylene dimerisation that is possible for a wide variety of radicals beyond just the phenyl radical (with β-styryl intermediate). The branching ratio of this vinylacetylene formation in the Bittner–Howard case is shown in Fig. 4(d). The maximum branching ratio of *ca.* 0.7% is achieved between 1500 and 1800 K and from pressures ranging from 5.33×10^2 to 10^6 Pa, with a somewhat weak dependence in this region. Though vinylacetylene production *via* this mechanism appears uncommon in the Bittner–Howard case, equivalent pathways for p-type alkyl radicals may be more likely and should not be ignored in future studies.

Key *trans*- and *cis*-Bittner–Howard pathways

Both the *trans*- and *cis*-Bittner–Howard pathways are present on the $C_{10}H_9$ landscape, have similar starting internal energies, and pathways for interconversion. Importantly, the inclusion of the *trans*-Bittner–Howard pathway measurably changes the distribution of products. The key pathways for both the *trans* and *cis* reactions must therefore be considered – particularly with regard to the most likely rearrangement between them.

The *trans*-Bittner–Howard pathways with the greatest contribution to our model are shown in Fig. 5. In prior studies, the *trans* addition to β-styryl radicals is either absent,[27] mentioned briefly,[24,25] or assumed to isomerise to the *cis* configuration with no explicit pathway provided.[5] However, the formation of *E*-styrylvinyl radicals (***E*-SVY**), as well as of the monocyclic $C_{10}H_8$ isomers ***E*-EPE** and 1-phenyl-2-vinylacetylene (**PVAC**), is competitive with the most favourable *cis* isomerisation pathway, which proceeds over t_{78}, i_{31} and t_{77} towards **NAPH** (shown in blue in Fig. 5). This *cis* isomerisation pathway is analogous to those shown in Fig. 1 for a variety of R-groups. The reaction rate across the transition states t_{77} and t_{78} is inhibited by their low density of states. Furthermore, the presence of two "gate-keeper" transition states rather than one significantly slows the

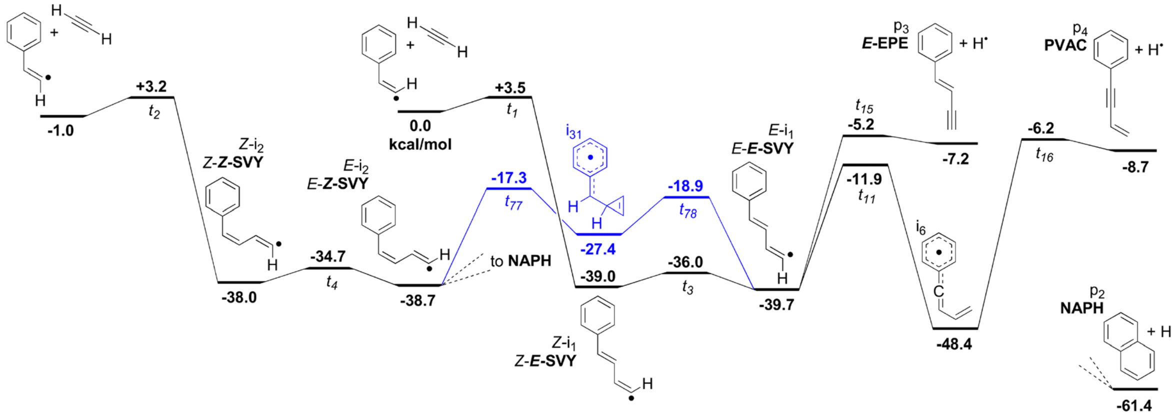
-1.0
+3.2
t_2
Z-i₂
Z-Z-SVY
-38.0
-34.7
t_4
E-i₂
E-Z-SVY
-38.7
to NAPH
0.0
kcal/mol
+3.5
t_1
-17.3
t_{77}
i₃₁
-27.4
-18.9
t_{78}
-39.0
-36.0
t_3
Z-i₁
Z-E-SVY
E-i₁
E-E-SVY
-39.7
-5.2
t_{15}
-11.9
t_{11}
p₃
E-EPE
+ H•
-7.2
i₆
-48.4
-6.2
t_{16}
p₄
PVAC
+ H•
-8.7
p₂
NAPH
+ H•
-61.4

Fig. 5 Selected pathways from the *trans* precursor towards the formation of **E-EPE**, **PVAC**, **VMBY** and **E-SVY**, as well as the most facile isomerisation to join to the *cis* surface. The *trans*/*cis* isomerisation pathway is shown in blue. **NAPH** is shown for comparison – see Fig. 6 for further detail.

rate of isomerisation from ***E*-SVY** to *Z*-2-styrylvinyl (***Z*-SVY**). If the isomerisation continues across t_{77} to the *cis* portion of the surface, however, return is unlikely, and the reaction proceeds similarly to the *cis* case.

The *cis* addition yields three pathways that lead to **NAPH** formation, presented in Fig. 6. Highlighted in red is a previously reported pathway.[25] The black pathways are competitive with the red pathway and are a source of both the **BZFV** and **NAPH** products. In particular, **BZFV** is an alternative product to the ring expansion pathway leading to **NAPH**. As discussed above, **BZFV** production maximises at moderate temperatures and low pressures, with a branching ratio of *ca.* 8% at 5.33×10^2 Pa and 1200 K. In contrast, **NAPH** production is most favoured at low temperature. This difference is attributed to a more relaxed (more loose) **BZFV** transition state (t_{67}), which has a strong positive temperature dependence. Though the **BZFV** branching ratio decreases above 1200 K, **NAPH** has a faster rate of relative decrease, such that **BZFV** is *ca.* 23% of **NAPH** production at 1800 K and 5.33×10^2 Pa. The overall decrease in **NAPH** and **BZFV** within only the *cis* addition pathway is the result of competition between redissociation and with formation of monocyclic $C_{10}H_8$ isomers, particularly ***Z*-EPE**.

Quantifying the significance of the *trans* pathway

To ascribe a value to the significance of the *trans*-vinyl radical addition chemistry within our model, the branching ratio for each species can be compared to when the *cis* reaction is alone considered. This leads to the following formula for the sum of absolute differences (SAD):

$$\mathrm{SAD} = \frac{1}{2}\sum_i |\phi_{i,\mathrm{mod}} - \phi_{i,cis}|$$

where i is the chemical species, $\phi_{i,\mathrm{mod}}$ is the modelled branching ratio averaged over both entry pathways, and $\phi_{i,cis}$ is the branching ratio of the *cis* reaction only. The prefactor of $\frac{1}{2}$ is included to avoid double-counting, since any decrease in the branching ratio at a particular species must lead to an equivalent increase over some combination of other species. The SAD is thus a value between 0 (no impact) and 1 (wholly dominant)

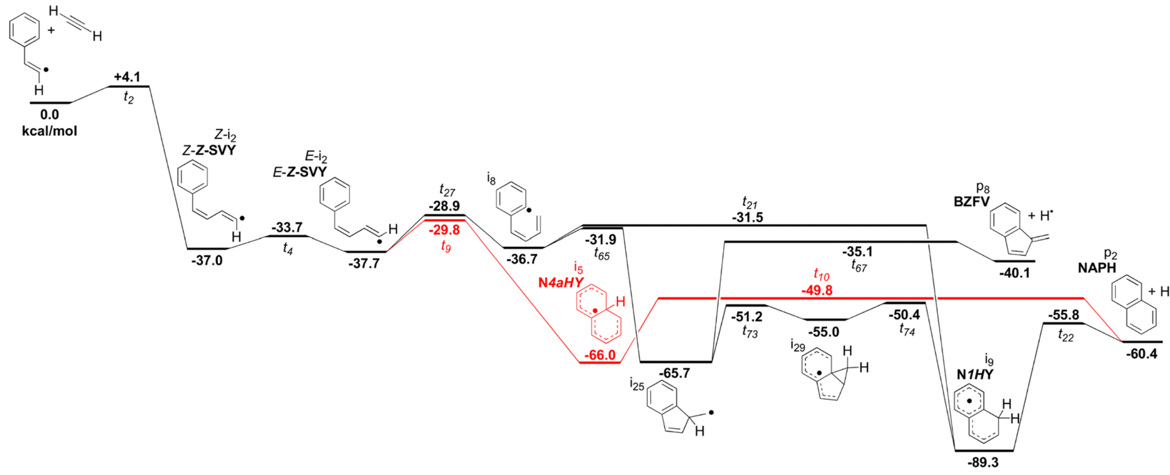
0.0
kcal/mol
+4.1
t_2
Z-i₂
Z-Z-SVY
-37.0
-33.7
t_4
E-i₂
E-Z-SVY
-37.7
t_{27}
-28.9
-29.8
t_9
i₈
-36.7
i₅
N4aHY
-66.0
-31.9
t_{65}
-65.7
i₂₅
t_{21}
-31.5
-35.1
t_{67}
t_{10}
-49.8
-51.2
t_{73}
-55.0
i₂₉
-50.4
t_{74}
p₈
BZFV
+ H•
-40.1
i₉
N1HY
-89.3
-55.8
t_{22}
p₂
NAPH
+ H•
-60.4

Fig. 6 Selected pathways from the *cis* precursor towards formation of **NAPH** and **BZFV**. The pathway modelled by Mebel *et al.*[25] is shown in red. Note that the *cis*-β-styryl radical is chosen as the reference energy, leading to slightly offset energies relative to Fig. 5.

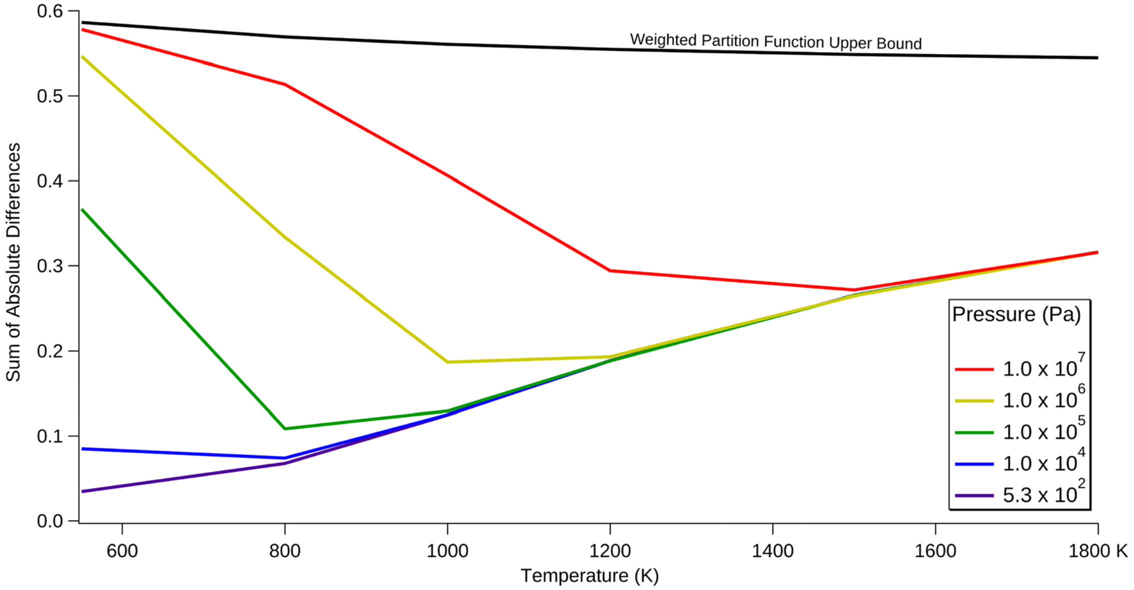

Fig. 7 Impact of the *trans* chemical pathways. The sum of absolute differences (SAD) as a function of pressure and temperature. The lower limit of the blue area is drawn at 5.33×10^2 Pa (4 torr). The weighted partition function upper bound depicts the maximum possible SAD (using the density-of-states weighting scheme between *trans* and *cis* starting points as discussed in the methods & model description).

and this quantifies the importance of including the *trans* pathway. In particular, comparing the combined model with the *cis*-only model accounts for the effects of the post-adduction surface as well as the relative probabilities of *trans* and *cis* addition.

Fig. 7 shows the SAD calculated for each temperature and pressure condition. The solid black line represents the maximum potential contribution of the *trans* reaction, assuming the *trans* reaction produces totally different products than the *cis* reaction. This upper bound is derived from the relative population of the *trans* and *cis* entry pathways, as calculated from the relative partition functions of the *trans* and *cis* transition states. The dotted black line represents a simpler model that ignores the molecular structure, instead only using the energetics of the separated *trans* and *cis* reactants. These bounds are discussed in more detail in the Methods & Model Description section. At all temperatures and pressures considered, the inclusion of the *trans* reaction significantly alters the branching ratios. The amount of change increases with increasing pressure, as earlier intermediates are quenched and stabilise such that this prevents the interconversion between *trans* and *cis* pathways. Increasing the temperature has a varying effect, depending on pressure. At the lowest pressures considered, increasing the temperature monotonically increases the effect of the *trans* reaction. This increase is attributed to the relatively low density of states of key transition states separating the *trans* and *cis* reactions, compared with competing pathways. Therefore, entropic effects cause *trans*/*cis* interconversion to be disfavoured.

At moderate to high pressures, increasing the temperature first decreases the SAD to the point where it approaches the lowest-pressure case, and then it increases in parallel with this lowest-pressure case. This inversion is possibly due to the decreasing efficiency of collisional deactivation as the temperature of the bath gas increases. Importantly, the *trans* reaction is most significant at 550 K and 10^7 Pa, in which it approaches the upper bound of 0.59. Almost all of this is attributed to collision-stabilised ***E*-SVY**. Even at atmospheric pressure the *trans* reaction has a SAD between 0.1 and 0.4 across all considered temperatures, with a maximum at the lowest temperature of 550 K. Thus, it is necessary to include the *trans* reaction when modelling the Bittner–Howard pathway, regardless of the pressure and temperature.

The SAD value is also useful for testing the robustness of the model to small changes in barrier height. This sensitivity analysis was performed at 1200 K and 10^5 Pa, corresponding to approximately the midpoint of the temperature and pressure parameters used in this work. By tweaking the energies of the "gatekeeper" transition states between the *trans* and *cis* pathways – that is, t_{77} and t_{78} – the change in the SAD can be measured. When the barrier heights of these transition states were lowered by 1 kcal mol^{-1}, the SAD decreased from 0.188 to 0.152. A 1 kcal mol^{-1} increase led to the SAD increasing to 0.229. In either case, the SAD remains the same order of magnitude, leaving the broader argument of this work unchanged. Therefore, while the quantitative values of the SAD may not be perfectly accurate, it can be concluded that the *trans* reaction must be included in models of aromatic molecular-weight growth chemistry pertinent to the primal stages of soot formation.

Conclusion

The Bittner–Howard pathway, despite its inclusion in HACA models for decades, has concealed complexity that has been underexplored in prior modelling literature. From this expanded modelling study, such pathways are expected to be most prominent at temperatures below 1600 K and pressures equal to or exceeding 10^5 Pa and these conditions correspond to the greatest quantity and variety of $C_{10}H_9$ radical isomers, including various RSRs. Furthermore, $C_{10}H_8$ comprises a greater diversity than previously described, even at moderate temperatures, including benzofulvene (**BZFV**) as well as 3 related monocyclic species: *E*- and *Z*-2-ethynyl-1-phenylethene (***E*-EPE** and ***Z*-EPE**), and 1-phenyl-2-vinylacetylene (**PVAC**). Though naphthalene (**NAPH**) is still the $C_{10}H_8$ isomer with the greatest branching ratio below 1800 K, other isomers are competitive from temperatures as low as 800–1000 K, much lower than predicted in earlier studies. Much of the difference can be attributed to the inclusion of *trans* chemistry in the model, which is most prominent at high pressure and low temperature – contributing the majority of the branching ratio at 550 K and pressures above 10^6 Pa. Even at the *least* favourable conditions for the relative contribution of the *trans* reaction, its inclusion still alters the predicted branching ratios by 4%.

Due to the similar ionisation energies of the most abundant predicted $C_{10}H_8$ isomers, experimental verification of the model presented in this work with photoionisation mass spectrometric techniques[44] may be challenging. Furthermore, increasing the temperature to encompass more of the model parameter space for the reaction of β-styryl radicals may allow for an enhanced identification of $C_{10}H_8$ isomers.

Finally, many of the *trans* pathways in the model, including the initial adduction step, do not strongly interact with the phenyl ring such that exchanging the phenyl group with different fundamental substituents results in generally similar energy landscapes, including the isomerisation pathway that connects with the *cis* reaction. The main differences arise when each radical R group is free, with energies correlated with the RSE of each. Radicals similar to the phenyl radical may therefore have similar acetylene addition reactions that are strongly affected by the inclusion of *trans*-Bittner–Howard-type pathways. Future Master Equation models of such systems should include these *trans* pathways. Ultimately, the impact of *trans*-vinyl radical intermediates on reactive radical chemistry demonstrates that they are necessary for the accurate modelling of combustion reactions and soot formation.

Data availability

The data supporting this article have been included as part of the ESI.†

Conflicts of interest

There are no conflicts to declare.

Acknowledgements

A. J. T., G. d. S. and S. J. B. acknowledge financial support for this research from the Australian Research Council (ARC) through the Discovery Project scheme (DP170101596 and DP240100612). The authors also acknowledge the generous allocation of computing resources by the NCI National Facility (Canberra, Australia) under Merit Allocation Scheme. P. D. K., J. A. T. and O. J. S. acknowledge receipt of an Australian Government Research Training Program Scholarship.

References

1 B. J. Finlayson-Pitts and J. N. PittsJr., Tropospheric air pollution: ozone, airborne toxics, polycyclic aromatic hydrocarbons, and particles, *Science*, 1997, **276**, 1045–1051.
2 K.-H. Kim, S. A. Jahan, E. Kabir and R. J. C. Brown, A review of airborne polycyclic aromatic hydrocarbons (PAHs) and their human health effects, *Environ. Int.*, 2013, **60**, 71–80.
3 I.-Y. L. Hsieh, G. P. Chossière, E. Gençer, H. Chen, S. Barrett and W. H. Green, An Integrated Assessment of Emissions, Air Quality, and Public Health Impacts of China's Transition to Electric Vehicles, *Environ. Sci. Technol.*, 2022, **56**, 6836–6846.
4 K. O. Johansson, M. P. Head-Gordon, P. E. Schrader, K. R. Wilson and H. A. Michelsen, Resonance-stabilized hydrocarbon-radical chain reactions may explain soot inception and growth, *Science*, 2018, **361**, 997–1000.
5 J. D. Bittner and J. B. Howard, Composition profiles and reaction mechanisms in a near-sooting premixed benzene/oxygen/argon flame, *Proc. Combust. Inst.*, 1981, **18**, 1105–1116.
6 M. Frenklach, D. W. Clary, W. C. Gardiner and S. E. Stein, Detailed kinetic modeling of soot formation in shock-tube pyrolysis of acetylene, *Proc. Combust. Inst.*, 1984, **20**, 887–901.
7 E. Reizer, B. Viskolcz and B. Fiser, Formation and growth mechanisms of polycyclic aromatic hydrocarbons: A mini-review, *Chemosphere*, 2022, **291**, 132793.
8 H. Jin, W. Yuan, W. Li, J. Yang, Z. Zhou, L. Zhao, Y. Li and F. Qi, Combustion chemistry of aromatic hydrocarbons, *Prog. Energy Combust. Sci.*, 2023, **96**, 101076.
9 V. V. Kislov, A. I. Sadovnikov and A. M. Mebel, Formation Mechanism of Polycyclic Aromatic Hydrocarbons beyond the Second Aromatic Ring, *J. Phys. Chem. A*, 2013, **117**, 4794–4816.
10 B. Jursic and Z. Zdravkovski, DFT study of the Diels–Alder reactions between ethylene with buta-1,3-diene and cyclopentadiene,*J. Chem. Soc., Perkin Trans. 2*, 1995, (6), 1223–1226.
11 R. P. Lindstedt and G. Skevis, Benzene formation chemistry in premixed 1,3-butadiene flames, *Proc. Combust. Inst.*, 1996, **26**, 703–709.
12 P. M. Woods, T. J. Millar, A. A. Zijlstra and E. Herbst, The Synthesis of Benzene in the Proto-planetary Nebula CRL 618, *Astrophys. J.*, 2002, **574**, L167.
13 J. A. Miller and S. J. Klippenstein, The Recombination of Propargyl Radicals and Other Reactions on a C_6H_6 Potential, *J. Phys. Chem. A*, 2003, **107**, 7783–7799.
14 F. Zhang, B. Jones, P. Maksyutenko, R. I. Kaiser, C. Chin, V. V. Kislov and A. M. Mebel, Formation of the Phenyl

Radical [$C_6H_5(X^2A_1)$] under Single Collision Conditions: A Crossed Molecular Beam and *ab Initio* Study, *J. Am. Chem. Soc.*, 2010, **132**, 2672–2683.

15 E. Wang and J. Ding, Reaction between the i-C_4H_5 radical and propargyl radical (C_3H_3): A theoretical study, *Chem. Phys. Lett.*, 2021, **768**, 138407.

16 E. Georganta, R. K. Rahman, A. Raj and S. Sinha, Growth of polycyclic aromatic hydrocarbons (PAHs) by methyl radicals: Pyrene formation from phenanthrene, *Combust. Flame*, 2017, **185**, 129–141.

17 X. Shi, Q. Wang and A. Violi, Reaction pathways for the formation of five-membered rings onto polyaromatic hydrocarbon framework, *Fuel*, 2021, **283**, 119023.

18 T. Yu and M. C. Lin, Kinetics of the phenyl radical reaction with ethylene: An RRKM theoretical analysis of low and high temperature data, *Combust. Flame*, 1995, **100**, 169–176.

19 A. B. Vakhtin, D. E. Heard, I. W. M. Smith and S. R. Leone, Kinetics of reactions of C_2H radical with acetylene, O_2, methylacetylene, and allene in a pulsed Laval nozzle apparatus at T = 103 K, *Chem. Phys. Lett.*, 2001, **344**, 317–324.

20 H. Jin, L. Ye, J. Yang, Y. Jiang, L. Zhao and A. Farooq, Inception of Carbonaceous Nanostructures *via* Hydrogen-Abstraction Phenylacetylene-Addition Mechanism, *J. Am. Chem. Soc.*, 2021, **143**, 20710–20716.

21 J. Zádor, M. D. Fellows and J. A. Miller, Initiation Reactions in Acetylene Pyrolysis, *J. Phys. Chem. A*, 2017, **121**, 4203–4217.

22 L. A. Singer and N. P. Kong, Vinyl Radicals. Stereoselectivity in Hydrogen Atom Transfer to Equilibrated Isomeric Vinyl Radicals, *J. Am. Chem. Soc.*, 1966, **88**, 5213–5219.

23 H. F. Piedra and M. Plaza, Photochemical halogen-bonding assisted generation of vinyl and sulfur-centered radicals: stereoselective catalyst-free C(sp^2)–S bond forming reactions, *Chem. Sci.*, 2023, **14**, 650–657.

24 V. V. Kislov, N. I. Islamova, A. M. Kolker, S. H. Lin and A. M. Mebel, Hydrogen Abstraction Acetylene Addition and Diels—Alder Mechanisms of PAH Formation: A Detailed Study Using First Principles Calculations, *J. Chem. Theory Comput.*, 2005, **1**, 908–924.

25 A. M. Mebel, Y. Georgievskii, A. W. Jasper and S. J. Klippenstein, Temperature- and pressure-dependent rate coefficients for the HACA pathways from benzene to naphthalene, *Proc. Combust. Inst.*, 2017, **36**, 919–926.

26 T. Yang, T. P. Troy, B. Xu, O. Kostko, M. Ahmed, A. M. Mebel and R. I. Kaiser, Hydrogen-Abstraction/Acetylene-Addition Exposed, *Angew. Chem., Int. Ed.*, 2016, **55**, 14983–14987.

27 T.-C. Chu, Z. J. Buras, M. C. Smith, A. B. Uwagwu and W. H. Green, From benzene to naphthalene: direct measurement of reactions and intermediates of phenyl radicals and acetylene, *Phys. Chem. Chem. Phys.*, 2019, **21**, 22248–22258.

28 A. E. Long, S. S. Merchant, A. G. Vandeputte, H.-H. Carstensen, A. J. Vervust, G. B. Marin, K. M. Van Geem and W. H. Green, Pressure dependent kinetic analysis of pathways to naphthalene from cyclopentadienyl recombination, *Combust. Flame*, 2018, **187**, 247–256.

29 L. Zhao, W. Lu, M. Ahmed, M. V. Zagidullin, V. N. Azyazov, A. N. Morozov, A. M. Mebel and R. I. Kaiser, Gas-phase synthesis of benzene *via* the propargyl radical self-reaction, *Sci. Adv.*, 2021, **7**, eabf0360.

30 J. Hanfeng, X. Lili, H. Junyu, Y. Jiuzhong, Z. Yan, C. ChuangChuang, P. Yang and A. Farooq, A chemical kinetic modeling study of indene pyrolysis, *Combust. Flame*, 2019, **206**, 1–20.

31 J. R. Barker, T. L. Nguyen, J. F. Stanton, C. Aieta, M. Ceotto, F. Gabas, T. J. D. Kumar, C. G. L. Li, L. L. Lohr, A. Maranzana, N. F. Ortiz, J. M. Preses, J. M. Simmie, J. A. Sonk and P. J. Stimac, *MultiWell-2020 Software Suite, K. R. Barker*, University of Michigan, Ann Arbor, Michigan, USA, 2020.

32 J. R. Barker, Multiple-Well, multiple-path unimolecular reaction systems. I. MultiWell computer program suite, *Int. J. Chem. Kinet.*, 2001, **33**, 232–245.

33 J. R. Barker, Energy transfer in master equation simulations: A new approach, *Int. J. Chem. Kinet.*, 2009, **41**, 748–763.

34 M. J. Frisch, G. W. Trucks, H. B. Schlegel, G. E. Scuseria, M. A. Robb, J. R. Cheeseman, G. Scalmani, V. Barone, G. A. Petersson, H. Nakatsuji, X. Li, M. Caricato, A. V. Marenich, J. Bloino, B. G. Janesko, R. Gomperts, B. Mennucci, H. P. Hratchian, J. V. Ortiz, A. F. Izmaylov, J. L. Sonnenberg, D. Williams-Young, F. Ding, F. Lipparini, F. Egidi, J. Goings, B. Peng, A. Petrone, T. Henderson, D. Ranasinghe, V. G. Zakrzewski, J. Gao, N. Rega, G. Zheng, W. Liang, M. Hada, M. Ehara, K. Toyota, R. Fukuda, J. Hasegawa, M. Ishida, T. Nakajima, Y. Honda, O. Kitao, H. Nakai, T. Vreven, K. Throssell, J. A. Montgomery, Jr., J. E. Peralta, F. Ogliaro, M. J. Bearpark, J. J. Heyd, E. N. Brothers, K. N. Kudin, V. N. Staroverov, T. A. Keith, R. Kobayashi, J. Normand, K. Raghavachari, A. P. Rendell, J. C. Burant, S. S. Iyengar, J. Tomasi, M. Cossi, J. M. Millam, M. Klene, C. Adamo, R. Cammi, J. W. Ochterski, R. L. Martin, K. Morokuma, O. Farkas, J. B. Foresman and D. J. Fox, *Gaussian 16 (Revision C.01)*, Gaussian, Inc., Wallingford CT, 2016.

35 G. da Silva, G3X-K theory: A composite theoretical method for thermochemical kinetics, *Chem. Phys. Lett.*, 2013, **558**, 109–113.

36 H. Hippler, J. Troe and H. J. Wendelken, Collisional deactivation of vibrationally highly excited polyatomic molecules. II. Direct observations for excited toluene, *J. Chem. Phys.*, 1983, **78**, 6709–6717.

37 T. Lenzer, K. Luther, K. Reihs and A. C. Symonds, Collisional energy transfer probabilities of highly excited molecules from kinetically controlled selective ionization (KCSI). II. The collisional relaxation of toluene: $P(E',E)$ and moments of energy transfer for energies up to 50 000 cm^{-1}, *J. Chem. Phys.*, 2000, **112**, 4090–4110.

38 D. L. Osborn, P. Zou, H. Johnsen, C. C. Hayden, C. A. Taatjes, V. D. Knyazev, S. W. North, D. S. Peterka, M. Ahmed and S. R. Leone, The multiplexed chemical kinetic photoionization mass spectrometer: a new approach to isomer-resolved chemical kinetics, *Rev. Sci. Instrum.*, 2008, **79**, 104103.

39 A. Kushnarenko, E. Miloglyadov, M. Quack and G. Seyfang, Intramolecular vibrational energy redistribution in $HCCCH_2X$ (X = Cl, Br, I) measured by femtosecond pump–probe experiments in a hollow waveguide, *Phys. Chem. Chem. Phys.*, 2018, **20**, 10949–10959.

40 S. Karmakar and S. Keshavamurthy, Intramolecular vibrational energy redistribution and the quantum ergodicity transition: a phase space perspective, *Phys. Chem. Chem. Phys.*, 2020, **22**, 11139–11173.

41 R. D. Levine, *Molecular Reaction Dynamics*, Cambridge University Press, Cambridge, 2005.

42 M. C. Smith, G. Liu, Z. J. Buras, T.-C. Chu, J. Yang and W. H. Green, Direct Measurement of Radical-Catalyzed C_6H_6 Formation from Acetylene and Validation of Theoretical Rate Coefficients for $C_2H_3 + C_2H_2$ and $C_4H_5 + C_2H_2$ Reactions, *J. Phys. Chem. A*, 2020, **124**, 2871–2884.

43 J. Hioe and H. Zipse, Radical Stability—Thermochemical Aspects, in *Encyclopedia of Radicals in Chemistry, Biology and Materials* ed. C. Chatgilialoglu and A. Studer, John Wiley & Sons, Ltd., 2012, Online, DOI: **10.1002/9781119953678.rad012**.

44 O. J. Shiels, M. B. Prendergast, J. D. Savee, D. L. Osborn, C. A. Taatjes, S. J. Blanksby, G. da Silva and A. J. Trevitt, Five *vs.* six membered-ring PAH products from reaction of o-methylphenyl radical and two C_3H_4 isomers, *Phys. Chem. Chem. Phys.*, 2021, **23**, 14913–14924.